Supplementary Information for

Highly Conductive and Stretchable Nanostructured Ionogels for 3D Printing Capacitive Sensors with Superior Performance

*Xiangnan He[1,2], Biao Zhang[3], Qingjiang Liu[1,2], Hao Chen[1,2], Jianxiang Cheng[1,2], Bingcong Jian[1,2], Hanlin Yin[1,2], Honggeng Li[1,2], Ke Duan[4], Jianwei Zhang[4], Qi Ge[1,2]**

[1] Shenzhen Key Laboratory of Soft Mechanics & Smart Manufacturing, Southern University of Science and Technology, Shenzhen, China.
[2] Department of Mechanical and Energy Engineering, Southern University of Science and Technology, Shenzhen 518055, China.
[3] Xi'an Institute of Flexible Electronics, Northwestern Polytechnical University, 127 West Youyi Road, Xi'an, China.
[4] Department of Materials Science and Engineering, College of Aerospace Science and Engineering, National University of Defense Technology.

*Corresponding author: Qi Ge, geq@sustech.edu.cn

This file includes:

Supplementary Text 1
Supplementary Figure 1 to 21
Supplementary Table 1 to 6
Supplementary Reference 1 to 3

Other Supplementary Materials for this manuscript include the following:

Supplementary Movie 1 to 5

Supplementary Text

1. Thermodynamic modeling on phase separation of the mixture of photopolymer and ionic liquid

The photopolymerization-induced phase separation of the mixture of benzyl acrylate (BA) and ionic liquid (IL) can be explained by the change the free energy ΔF_{mix} which can be expressed by the Flory-Huggins equation [1]:

$$\Delta F_{\mathrm{mix}} = \Delta U_{\mathrm{mix}} - T\Delta S_{\mathrm{mix}} = \underbrace{kT\chi\phi(1-\phi)}_{\Delta U_{\mathrm{mix}}} + \underbrace{kT\left[\frac{\phi}{N_{\mathrm{I}}}\ln\phi + \frac{1-\phi}{N_{\mathrm{P}}}\ln(1-\phi)\right]}_{-T\Delta S_{\mathrm{mix}}} \quad \text{(S1)}$$

where ΔU_{mix} is mixing enthalpy; ΔS_{mix} is mixing entropy; k is Boltzmann constant; T is absolute temperature; χ is Flory interaction parameter between ILs and the surrounding monomers or polymer networks; ϕ is the mixing ratio of IL; N_{I} and N_{P} are the degrees of polymerizations of IL and BA. For IL, $N_{\mathrm{I}} = 1$ as it is not polymerized. For BA, $N_{\mathrm{P}} = 1$ before photopolymerization; and $N_{\mathrm{P}} > 1000$ after photopolymerization.

When the two species are miscible, ΔF_{mix} must be negative. Because no phase separation is observed for the BA-IL mixture solution, the initial ΔF_{mix} is negative. Photopolymerization makes N_{P} increase more than 1000 times, so that $-T\Delta S_{\mathrm{mix}}$ increases significantly, which leads to a positive ΔF_{mix}. Therefore, phase separation occurs.

In the Flory-Huggins equation which is derived by the simplified lattice model, the Flory interaction parameter χ can be modeled as

$$\chi \equiv \frac{z}{2}\frac{(u_{P-I} - u_{I-I} - u_{P-P})}{kT} \quad \text{(S2)}$$

where z is the coordination number of the lattice and $z = 6$ for the 3D case; $u_{\mathrm{I\text{-}I}}$, $u_{\mathrm{P\text{-}P}}$ and $u_{\mathrm{P\text{-}I}}$ are interaction energies between adjacent lattice sites occupied by the two

species ($u_{\text{I-I}}$: interaction energy between IL and IL; $u_{\text{P-P}}$: interaction energy between polymer to polymer; $u_{\text{P-I}}$: interaction energy between polymer to IL). after adding sufficient poly(ethylene glycol) methyl ether methacrylate (PEGMA) into the polymer network, the polyethylene oxide (PEO) side chains on PEGMA greatly facilitate the interaction between polymer network and ionic liquid [2, 3], so that the interaction energy between polymer and IL $u_{\text{P-I}}$ decreases significantly. The sharp reduction in $u_{\text{P-I}}$ leads to a much lower χ so that the mixing enthalpy ΔU_{mix}, which ensures a negative ΔF_{mix} and the miscibility between the polymer network and IL.

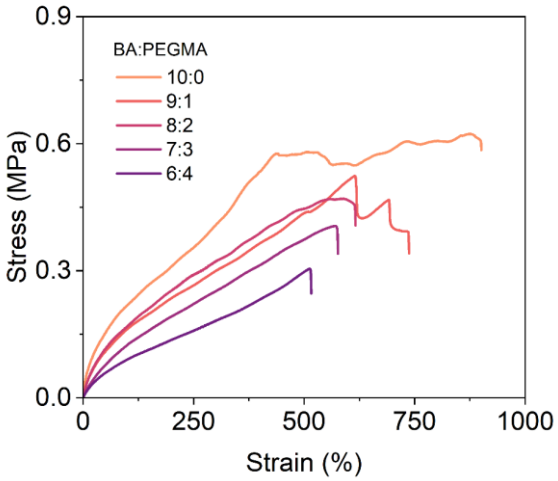

Supplementary Figure 1. Effect of PEGMA content on mechanical properties. Stress-strain behavior of the CSN ionogel with different PEGMA contents.

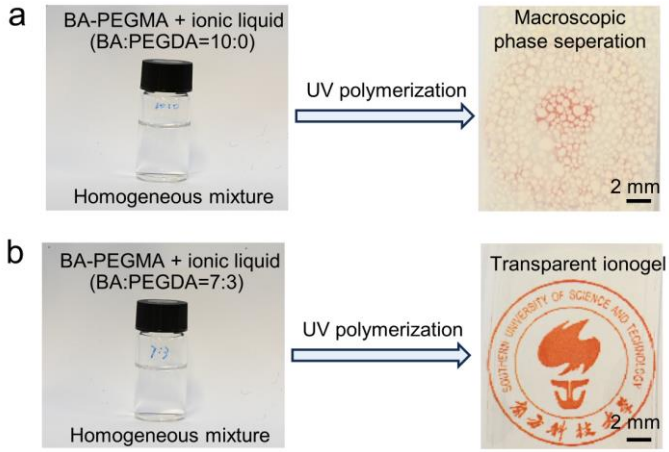

Supplementary Figure 2. The photographs of the BA-PEGMA ionogel with different BA:PEGMA ratios before and after UV polymerization. a BA:PEGMA = 10:0. **b** BA:PEGMA = 7:3.

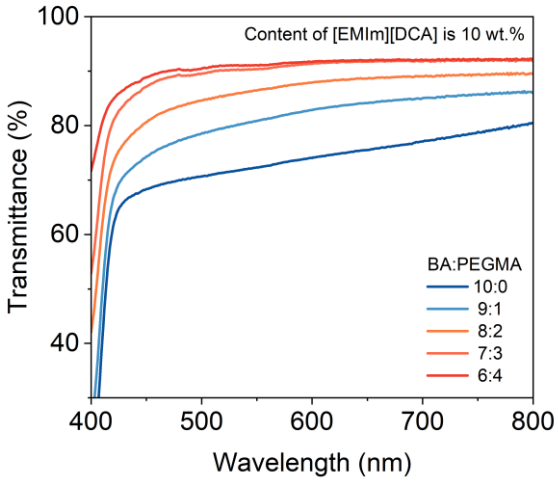

Supplementary Figure 3. The transparency of ionogels. Transmittance versus wavelength curves of ionogel with different proportions of BA:PEGMA. Samples for testing were 1 mm thick.

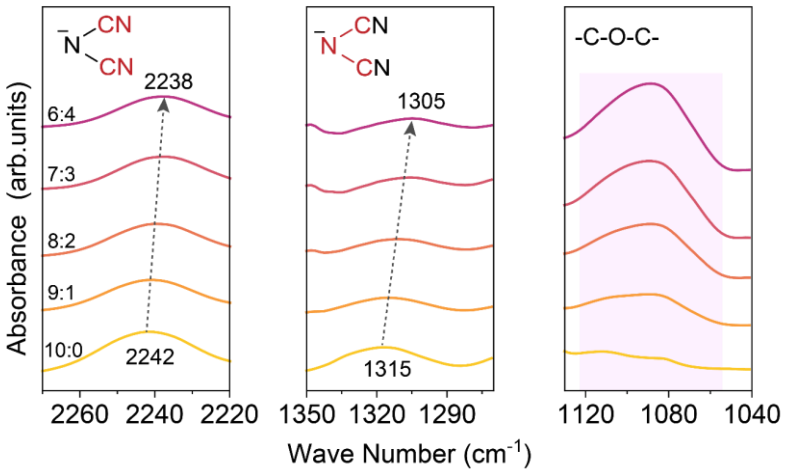

Supplementary Figure 4. The interaction between polymer network and ionic liquid. FTIR spectrum of the ionogels with different PEGMA contents.

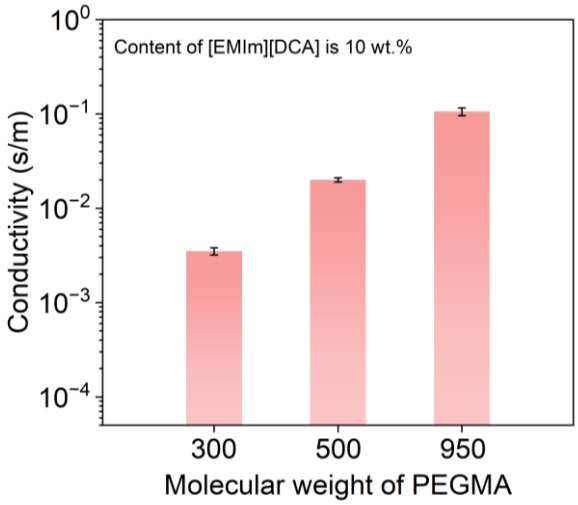

Supplementary Figure 5. Effect of PEGMA molecular weights on conductivity. Ionic conductivity of the ionogel with different molecular weights of PEGMA. 950, 500 and 300 represent the molecular weight of PEO chain. Data are presented as the mean values ± SD, n = 3 independent samples. Source data are provided as a Source Data file.

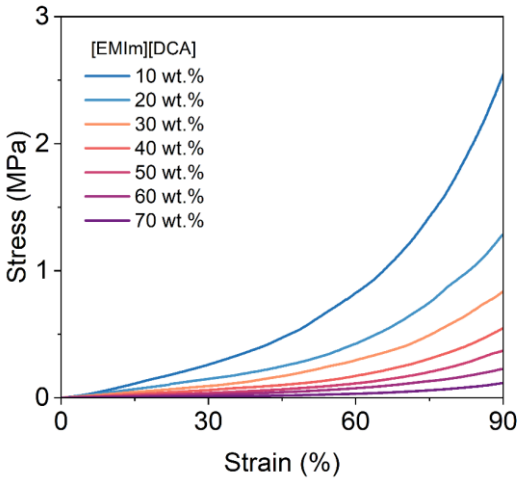

Supplementary Figure 6. Effect of [EMIm][DCA] content on mechanical properties. Compressive test of the ionogels with different [EMIm][DCA] contents.

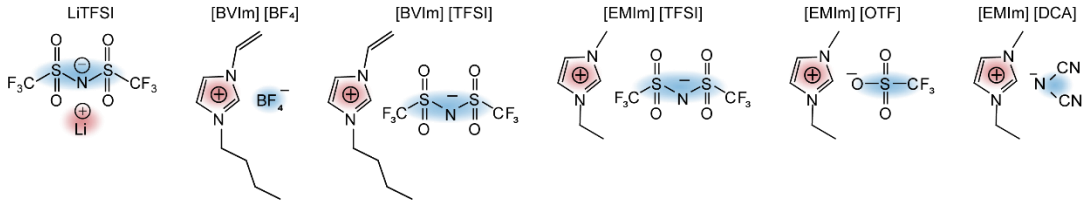

Supplementary Figure 7. Different conductive component. Detailed chemical structures of LiTFSI, [BVIm][BF4], [BVIm][TFSI], [EMIm][TFSI], [EMIm][OTF] and [EMIm][DCA].

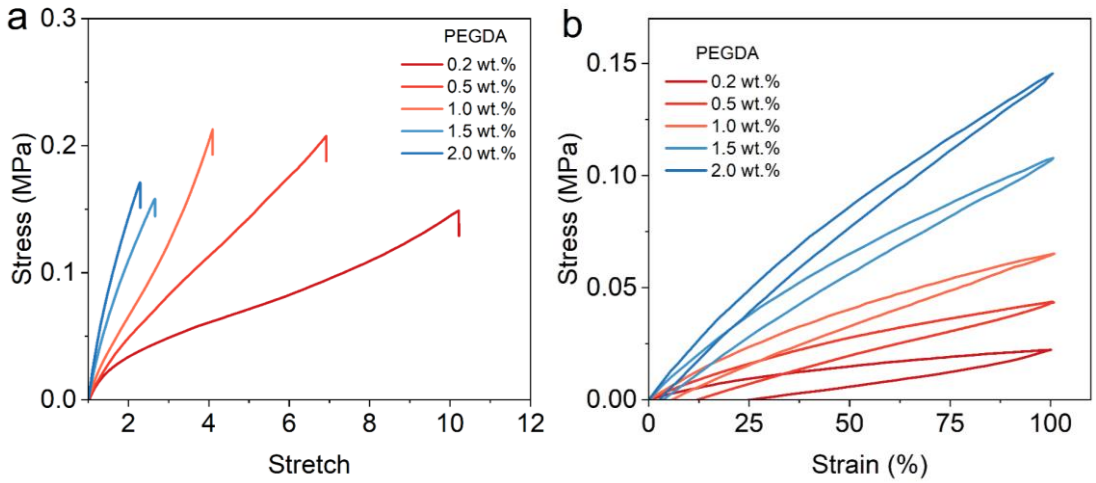

Supplementary Figure 8. Effect of PEGDA content on mechanical properties of CSN ionogels. a Stress–strain behavior of the CSN ionogel with different PEGDA content. **b** Cyclic stress-strain curves of the CSN ionogel with different PEGDA content.

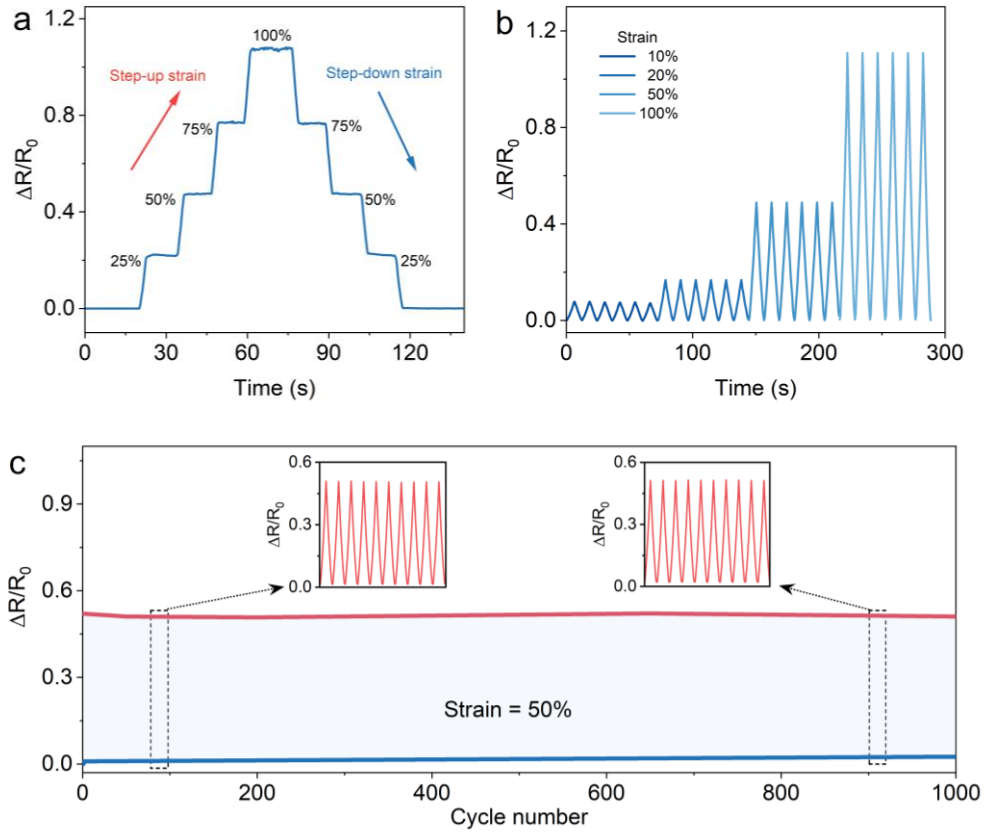

Supplementary Figure 9. Sensing performance of the strain sensor based CSN ionogels. a One cycle of strain sensing performance characterization from 0% to 25%, 50%, 75%, and 100%, and then back to 0%. **b** Dynamic cyclic tests with different amplitude of tensile strains. **c** Cycling stability at a strain of 50% within 1000 cycles.

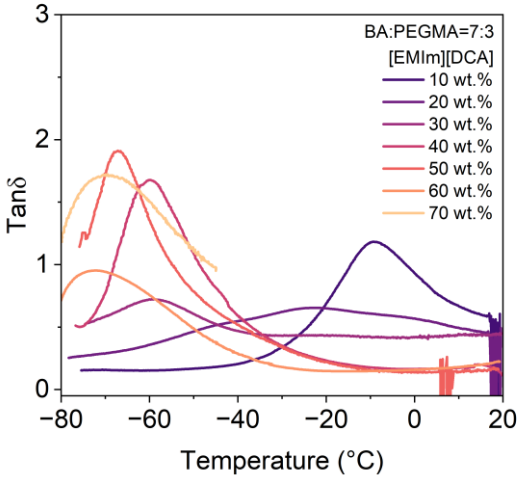

Supplementary Figure 10. Effect of [EMIm][DCA] content on T_g. Tanδ-temperature curves of the ionogels with various proportions of [EMIm][DCA] by DMA tests.

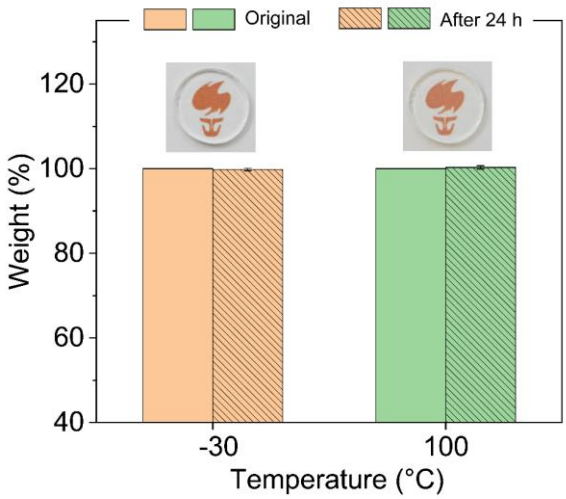

Supplementary Figure 11. Thermal stability of ionogels. Weight change of ionogel samples after being stored at 100℃ and -30℃ for 24 h. Data are presented as the mean values ± SD, $n = 3$ independent samples. Source data are provided as a Source Data file.

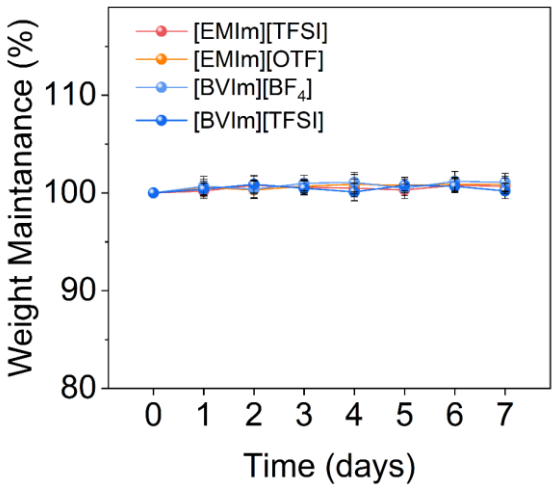

Supplementary Figure 12. Effect of humidity on ionogels. Weight change of the P(BA-*co*-PEGMA) samples with different ionic conductive component in humid environments. Data are presented as the mean values ± SD, $n = 3$ independent samples. Source data are provided as a Source Data file.

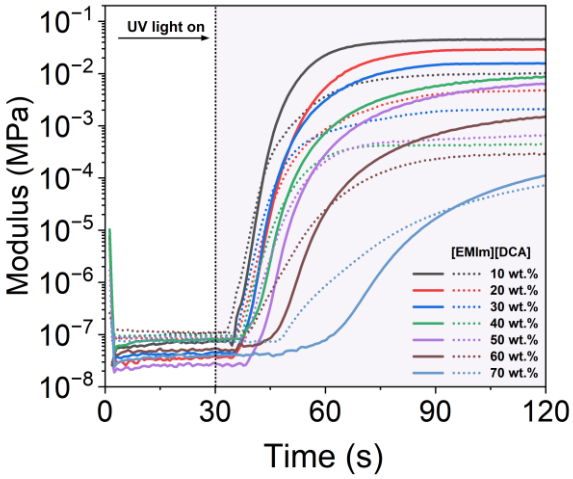

Supplementary Figure 13. Effect of [EMIm][DCA] contents on photorheological properties. Photorheology curves during light exposures of CSN ionogel precursor solution with different content of [EMIm][DCA]. (Solid curve: storage modulus, Dotted curve: loss modulus).

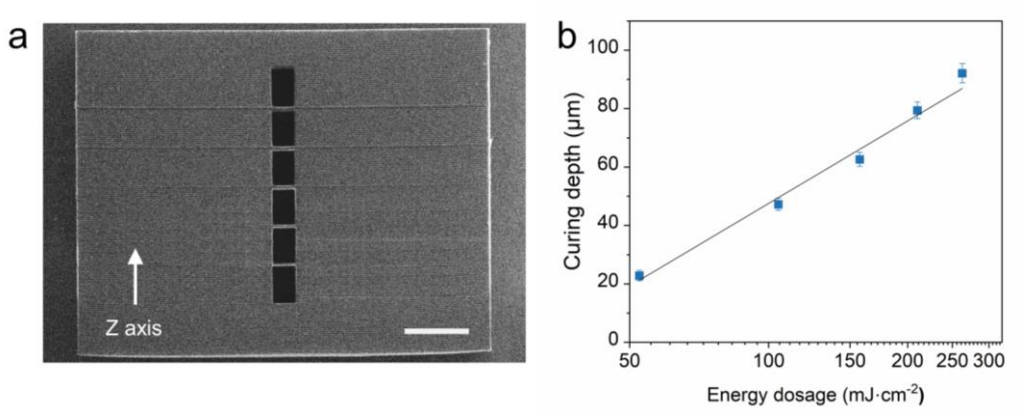

Supplementary Figure 14. Characterizations on printing resolution in vertical directions. a SEM image of the sample for curing depth study. Scale bar: 300 μm. **b** Energy dosage on curing depth (light source: 405 nm, 52.6 mW/cm^2). Data are presented as the mean values ± SD, n = 3 independent samples. Source data are provided as a Source Data file.

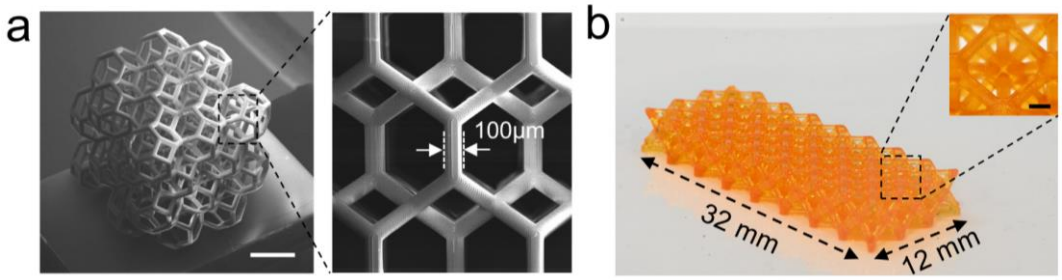

Supplementary Figure 15. 3D printed structures with CSN ionogel. **a** SEM image of a Kelvin foam structure. Scale bar: 1 mm. **b** An Octet truss structure. Scale bar: 1 mm.

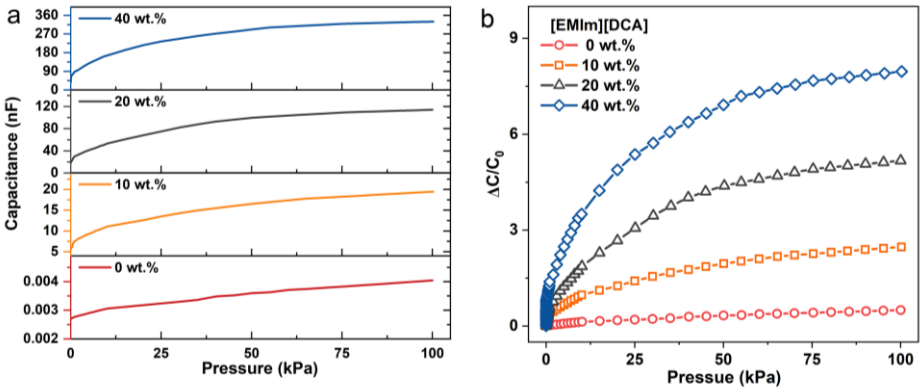

Supplementary Figure 16. **Effect of [EMIm][DCA] content on performance of CSN ionogel capacitive sensors. a** Comparisons of the performance of CSN ionogel capacitive sensors with different contents [EMIm][DCA]. **b** Comparison of pressure sensitivities of CSN ionogel capacitive sensors with different contents [EMIm][DCA].

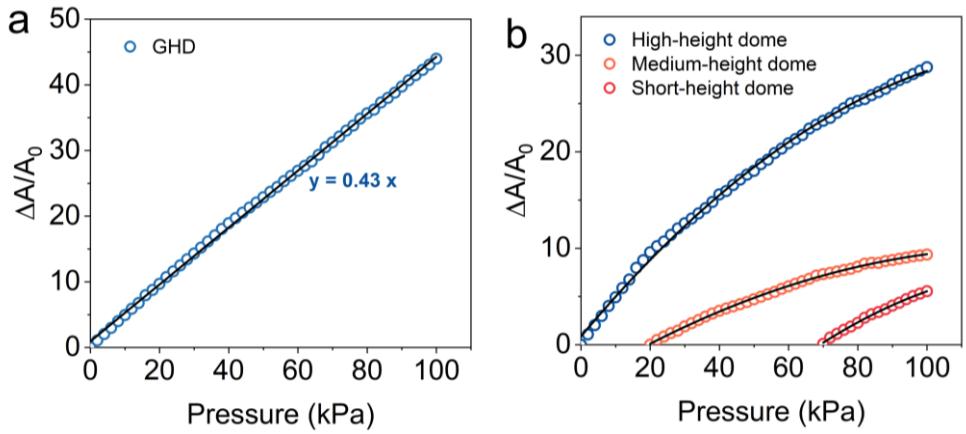

Supplementary Figure 17. Sensing mechanism of CSN ionogel capacitive sensor with gradient-height domes (GHD). a Normalized change in contact area change for the dielectric layers with GHD structure under pressures over 100 kPa. **b** Normalized change in contact area change for three height domes (high-height dome: $y_1 = -0.0015\ x^2 + 0.43\ x$, medium-height dome: $y_2 = -0.0085\ x^2 + 0.22\ x$, short-height dome: $y_3 = -0.0016\ x^2 + 0.46\ x$).

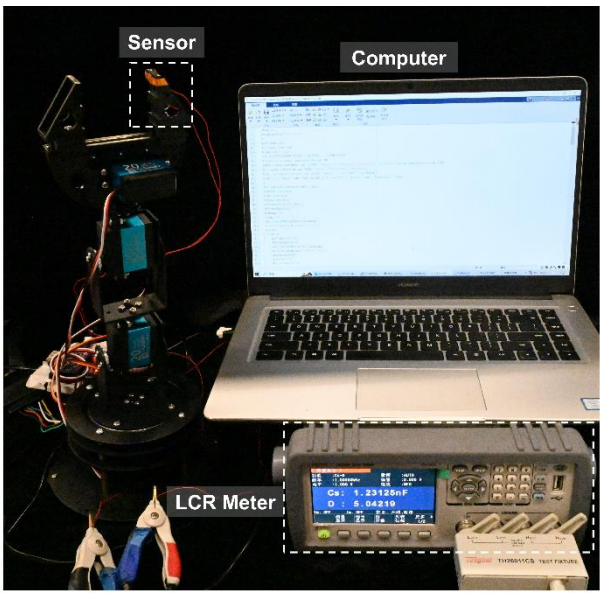

Supplementary Figure 18. Robotic hand-sensor integration. Photograph of the control system for robotic hand integrated with a 3D printed sensor.

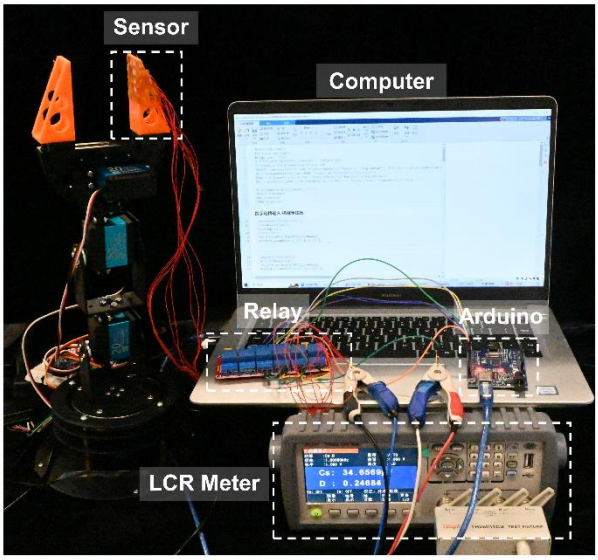

Supplementary Figure 19. Robotic hand-sensor array integration. Photograph of the control system for robotic hand integrated with a sensor array consisting of five sensors.

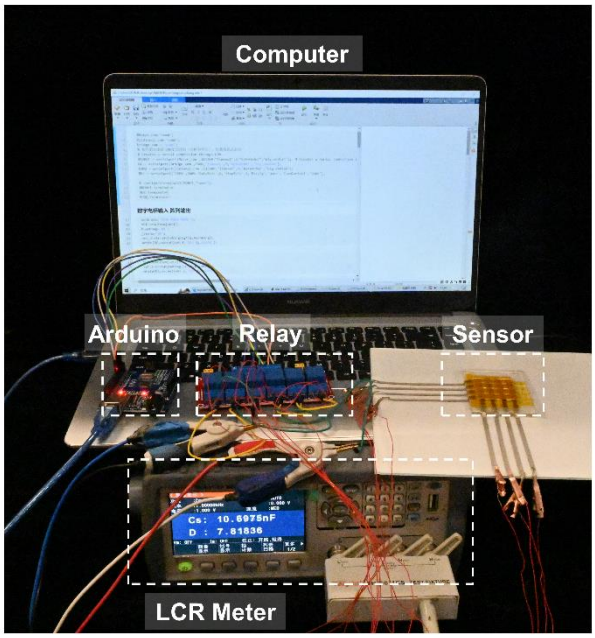

Supplementary Figure 20. Multiplex pressure sensor array. Photograph of the control system for a multiplex pressure sensor array with 4 × 4 sensing pixels.

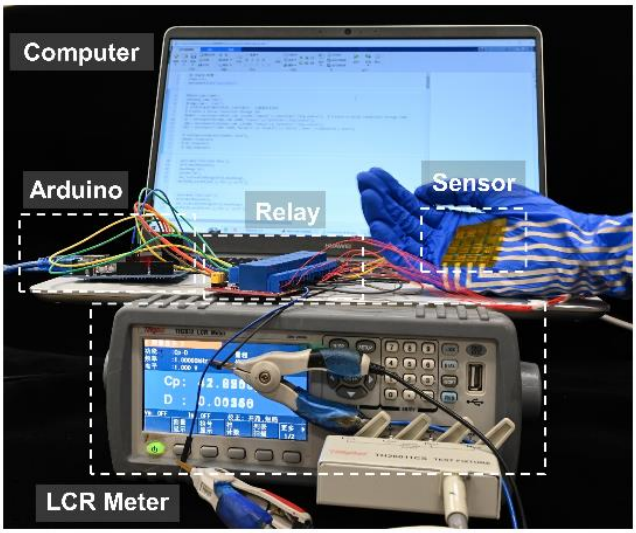

Supplementary Figure 21. Multiplex pressure sensor array on the glove. Photograph of the control system for a multiplex pressure sensor array with 4 × 4 sensing pixels on a glove.

Supplementary Table 1. Comparison of the ionogel in this work with previously reported.

Reference No. in the main text	Elongation-at-break (%)	Ionic conductivity (S/m)	3D printability	Printing resolution (μm)	Type of Sensor
This work	**1580**	**3.23**	**Yes**	**5**	Capacitive-pressure
[11]	2000	0.1	Yse	N.R.	Capacitive-pressure
[27]	1045	0.58	Yes	~ 1000	Resistance-strain
[28]	10	0.03	Yes	~ 1000	N.A.
[29]	487	0.015	Yes	~ 1000	Resistance-strain
[30]	/	0.12	Yes	~ 1000	N.A.
[31]	7000	0.11	Yes	N.R.	Resistance-strain
[32]	500	0.3	Yes	~ 1000	Resistance-strain
[33]	28	0.54	Yes	200	N.A.
[39]	1400	0.025	Yes	N.R.	Resistance-strain
[40]	10000	0.01	Yes	~ 1000	Capacitance-strain
[41]	600	0.078	Yes	~ 1000	Resistance-strain
[42]	2580	0.042	No	N.A.	Capacitance-strain
[43]	1312	0.12	No	N.A.	Capacitive-pressure
[44]	2066	0.29	No	N.A.	Resistance-strain
[45]	1100	0.21	Yes	N.R.	Resistance-strain
[46]	6000	0.024	No	N.A.	Resistance-strain
[47]	600	0.1	No	N.A.	N.A.
[48]	5000	0.007	No	N.A.	N.A.

N.A.: not applicable; N.R.: not reported.

Supplementary Table 2. The compositions of various copolymer ionogels.

	BA (wt.%)	PEGMA (wt.%)	[EMIm][DCA] (wt.%)	TPO (wt.%)	PEGDA (wt.%)
BA:PEGMA=10:0	88.80	0.00	10.0	1.0	0.2
BA:PEGMA=9:1	79.92	8.88	10.0	1.0	0.2
BA:PEGMA=8:2	71.04	17.76	10.0	1.0	0.2
BA:PEGMA=7:3	62.16	26.64	10.0	1.0	0.2
BA:PEGMA=6:4	53.28	35.52	10.0	1.0	0.2

Supplementary Table 3. The compositions copolymer ionogels with different molecular weights PEGMA in same molar concentration.

Molecular Weight (g/mol)	BA (g)	PEGMA (g)	[EMIm][DCA] (g)	TPO (g)	PEGDA (g)
M_n=950	62.16	26.64	10.0	1.0	0.2
M_n=500	62.16	14.02	10.0	1.0	0.2
M_n=300	62.16	8.41	10.0	1.0	0.2

Supplementary Table 4. The compositions of copolymer ionogels with various [EMIm][DCA] content.

	BA (wt.%)	PEGMA (wt.%)	[EMIm][DCA] (wt.%)	TPO (wt.%)	PEGDA (wt.%)
1	62.16	26.64	10.0	1.0	0.2
2	55.16	23.64	20.0	1.0	0.2
3	48.16	20.64	30.0	1.0	0.2
4	41.16	17.64	40.0	1.0	0.2
5	34.16	14.64	50.0	1.0	0.2
6	27.16	11.64	60.0	1.0	0.2
7	20.16	8.64	70.0	1.0	0.2

Supplementary Table 5. The compositions of copolymer ionogels with various conductive component.

	BA (wt.%)	PEGMA (wt.%)	Conductive component (wt.%)	TPO (wt.%)	PEGDA (wt.%)
LiTFSI	55.16	23.64	20.0	1.0	0.2
[BVIm][BF_4]	55.16	23.64	20.0	1.0	0.2
[BVIm][TFSI]	55.16	23.64	20.0	1.0	0.2
[EMIm][TFSI]	55.16	23.64	20.0	1.0	0.2
[EMIm][OTF]	55.16	23.64	20.0	1.0	0.2
[EMIm][DCA]	55.16	23.64	20.0	1.0	0.2

Supplementary Table 6. The compositions of copolymer ionogels with various PEGDA content.

	BA (wt.%)	PEGMA (wt.%)	[EMIm][DCA] (wt.%)	TPO (wt.%)	PEGDA (wt.%)
1	41.16	17.64	40.0	1.0	0.2
2	40.95	17.55	40.0	1.0	0.5
3	40.60	17.40	40.0	1.0	1.0
4	40.25	17.25	40.0	1.0	1.5
5	39.90	17.10	40.0	1.0	2.0

Supplementary References

1. Michael Rubinstein, Colby RH. *Polymer physics*. Oxford University Press (2003).
2. Schulze MW, McIntosh LD, Hillmyer MA, Lodge TP. High-modulus, high-conductivity nanostructured polymer electrolyte membranes via polymerization-induced phase separation. *Nano Letters* **14**, 122-126 (2014).
3. Chopade SA, So SY, Hillmyer MA, Lodge TP. Anhydrous proton conducting polymer electrolyte membranes via polymerization-induced microphase separation. *ACS Applied Materials & Interfaces* **8**, 6200-6210 (2016).